JACS DIRECTORY Hosting Innovations

Share Your Innovations through JACS Directory

Journal of Advanced Chemical Sciences

Visit Journal at http://www.jacsdirectory.com/jacs



DFT Calculations, Docking, Antioxidant and Anticancer Activity of Mononuclear Nickel(II) Complexes

K. Mancha Madha, N. Ramalakshmi*

Post Graduate and Research Department of Chemistry, Presidency College (Autonomous), Chennai - 600 005, Tamil Nadu, India.

ARTICLE DETAILS

Article history: Received 05 May 2017 Accepted 25 May 2017 Available online 29 July 2017

Keywords: Schiff Base Ligands DFT Calculations Antimicrobial DPPH Radicals Anticancer Activity

ABSTRACT

A series of mononuclear nickel(II) complexes (1–6) have been synthesized from substituted salicylaldehydes containing Schiff bases and characterized by varies spectral methods. The structural parameters of the complexes were evaluated by UV-Vis and DFT calculations, and results indicates square pyramidal (1–3) and octahedral (4–6) geometry around nickel(II) ion. Antimicrobial activity of the complexes exhibits moderate activity, which also exhibit better scavenging activity against ABTS and DPPH methods. In the molecular docking studies, the complexes are showed π – π , σ – π , hydrogen bonding, van der Waals and electrostatic interactions with EGFR kinase receptor. The nickel(II) complexes 2 and 5 show better anticancer activity against MDA-MB-231 cell lines compared to cisplatin and other complexes.

1. Introduction

The 'privileged ligands' (Schiff base ligands) play a vital role in coordination chemistry due to their willingness in coordination with many transition metal ions and easily form a highly stable complexes. Notably, the complexes of Schiff base ligands show good antibacterial, antifungal, antioxidant, anti-inflammatory, antimalarial, antiviral, antitubercular, hypothermic, hypertensive and anticancer activities [1–4]. Recently, a verity of tridentate Schiff base complexes display potential application in the area of industrial and analytical fields such as dyes, pigments and as catalysts in varies reaction such as reduction reaction of ketones, polymerization reaction, oxidation of organic compounds, reduction of thionyl chloride, Henry reaction, aldol reaction, epoxidation of alkenes, hydrosilylation of ketones, synthesis of bis(indolyl)methanes and Diels-Alder reaction [5–7]. Compare to organic ligands, the corresponding complexes show better activity in various fields due to their chelating behaviour and structural aspects [8].

The first metal-based anticancer drug cisplatin was discovered in the year of 1965, which cures 95% ovarian and testicular cancers. And also, other platinum-based anticancer drugs such as carboplatin, oxaliplatin and nedaplatin have been developed and cure variety of cancers. However, the uses of these platinum based drugs are associated with severe toxicity, side effects, low water solubility and drug resistance. To overcome these drawbacks, many researchers focus to develop other platinum based transition metal complexes with improved anticancer activity and less toxicity. In this connection, a variety of nickel(II) complexes were designed and developed, and tested against various cancer cell lines [9–11]. Based on the above facts, we have opted to synthesis salicylaldehydes containing Schiff base ligands and their mononuclear nickel(II) complexes and studied their spectral, DFT calculation, antibacterial, antioxidant, docking and anticancer properties.

2. Experimental Methods

2.1 Materials

Diethylenetriamine, triethylenetetraamine, salicylaldehydes, 5-methylsalicylaldehyde and 5-bromosalicylaldehyde were purchased from

*Corresponding Author Email Address: ggchemrsch@gmail.com (N. Ramalakshmi) Sigma-Aldrich (USA). Analytical grade of solvents were purchased from AVRA and E. Merck, and used as received without further purification. Tetra(n-butyl)ammonium perchlorate (TBAP) was purchased from Fluka (Switzerland), which used as the supporting electrolyte in the electrochemical measurements. The NiCl₂-6H₂O salt was purchased from Merck. The ligands (L^{1-6}) were synthesized from previously reported procedure [12].

2.2 Physical Measurements

Elemental analysis (CHN) of the complexes was carried out with a Perkin-Elmer 240 elemental analyser. Vibrational spectra were recorded on a Shimadzu model IR-Affinity-1 spectrophotometer using KBr disc technique in the range of 4000– $400~cm^{-1}$. Electronic absorption spectra were recorded using a Perkin-Elmer Lambda 35 double beam spectrophotometer. Electro spray ionization (ESI) mass spectra were recorded on Q-Tof mass spectrometer using acetonitrile as a medium. Cyclic voltammograms were recorded on a CHI-602D (CH Instruments Co., USA) electrochemical analyzer using a three-electrode cell in which a glassy carbon electrode was the working electrode, a saturated Ag/AgCl electrode was the reference electrode and platinum wire was used as the auxiliary electrode. TBAP was used as the supporting electrolyte (0.1 M) and all complex solutions were around $10^{-3}~\rm M$ concentration. X-Band EPR spectra of complexes were recorded on Varian EPR-E 112 spectrometer at room temperature.

2.3 General Procedure for Synthesis of Mononuclear Nickel(II) Complexes (1-6)

All the nickel(II) complexes (1–6) were synthesized using the similar procedure as given below: A methanolic solution (30 mL) of Schiff base ligand (L^{1-6} , 1 mmol) and NiCl₂.6H₂O (0. 13 g, 1 mmol) was stirred at room temperature for 2 h, and the reaction was carried out for 6 h under reflux, and the reaction mixture was filtered hot and kept aside for slow evaporation. The resulting product was washed with diethyl ether and dried in vacuum. Attempts taken to obtain single crystal but for all the complexes went unsuccessful.

2.3.1 [Ni(L1)] (1)

Yield: 0.33 g (89.66%). Colour: Yellowish brown. Anal. Calc. for: $C_{18}H_{19}N_3O_2Ni$ (368.06): C, 58.74; H, 5.20; N, 11.42. Found: C, 58.80; H, 5.16; N, 11.36%. Selected IR data (KBr, υ/cm^{-1}): 1618 $\upsilon(C=N)$, 1385 $\upsilon(Ar-O)$,

1591 $\upsilon(N-H)$. UV-Vis (DMF): λ/nm : 241 $(\pi-\pi^*)$ (31,640), 342 $(n-\pi^*)$ (10,400), 640 (d-d) (290). ESI-MS (m/z): 367.08 $[Ni(L^1)]^*$.

2.3.2 [Ni(L2)] (2)

Yield: 0.35 g, (88.35%). Colour: Yellowish brown. Anal. Calc. for: $C_{20}H_{23}N_3O_2Ni$ (396.11): C, 60.64; H, 5.85; N, 10.61. Found: C, 60.52; H, 5.89; N, 10.57%. Selected IR data (KBr, υ/cm^{-1}): 1620 $\upsilon(C=N)$, 1391 $\upsilon(Ar-O)$, 1581 $\upsilon(N-H)$. UV-Vis (DMF): λ/nm : 244 $(\pi-\pi^*)$ (31,700), 347 $(n-\pi^*)$ (10,610), 639 (d–d) (300). ESI-MS (m/z): 395.11 [Ni(L²)]+.

2.3.3 [Ni(L3)] (3)

Yield: 0.47 g, (89.38%). Colour: Yellowish brown. Anal. Calc. for: $C_{18}H_{17}Br_2N_3O_2Ni$ (525.85): C, 41.11; H, 3.26; N, 7.99. Found: C, 41.13; H, 3.30; N, 7.88%. Selected IR data (KBr, υ/cm^{-1}): 1622 $\upsilon(C=N)$, 1387 $\upsilon(Ar-O)$, 1583 $\upsilon(N-H)$. UV-Vis (DMF): λ/nm : 262 $(\pi-\pi^*)$ (31,900), 352 $(n-\pi^*)$ (10,780), 651 (d-d) (310). ESI-MS (m/z): 522.90 [Ni(L³)]*.

2.3.4 [Ni(L4)] (4)

Yield: 0.39 g, (94.86%). Colour: Yellowish brown. Anal. Calc. for: $C_{20}H_{24}N_4O_2Ni$ (411.12): C, 58.43; H, 5.88; N, 13.63. Found: C, 58.36; H, 5.89; N, 13.65%. Selected IR data (KBr, υ/cm^{-1}): 1619 $\upsilon(C=N)$, 1389 $\upsilon(Ar-O)$, 1578 $\upsilon(N-H)$. UV-Vis (DMF): λ/nm : 264 ($\pi-\pi^*$) (32,110), 356 ($n-\pi^*$) (10,710), 638 (d-d) (320), 924 (d-d) (075). ESI-MS (m/z): 410.13 [Ni(L⁴)]+.

2.3.5 [Ni(L5)] (5)

Yield: 0.39 g, (88.80%). Colour: Yellowish brown. Anal. Calc. for: $C_{22}H_{28}N_4O_2Cu$ (439.18): C, 60.17; H, 6.43; N, 12.76. Found: C, 60.19; H, 6.37; N, 12.68%. Selected IR data (KBr, υ/cm^{-1}): 1630 $\upsilon(C=N)$, 1386 $\upsilon(Ar-O)$, 1594 $\upsilon(N-H)$. UV-Vis (DMF): λ/nm : 271 ($\pi-\pi^*$) (32,020), 359 ($n-\pi^*$) (11,000), 641 (d-d) (315), 921 (d-d) (065). ESI-MS (m/z): 438.16 [Ni(L⁵)]*.

2.3.6 [Ni(L6)] (6)

Yield: 0.48 g, (84.37%). Colour: Yellowish brown. Anal. Calc. for: $C_{20}H_{22}Br_2N_4O_2Ni$ (568.92): C, 42.22; H, 3.90; N, 9.85. Found: C, 42.28; H, 3.93; N, 9.81%. Selected IR data (KBr, υ/cm^{-1}): 1631 $\upsilon(C=N)$, 1394 $\upsilon(Ar-O)$, 1589 $\upsilon(N-H)$. UV-Vis (DMF): λ/nm : 259 $(\pi-\pi^*)$ (32,020), 360 $(n-\pi^*)$ (11,430), 647 (d-d) (345), 917 (d-d) (80). ESI-MS (m/z): 565.95 [Ni(L⁶)]*.

2.4 Computational Details

The complexes were optimized by using Gaussian 03 software package [13]. The quantum chemical calculations were performed applying DFT method with Becke-3-Lee-Yang-Parr (B3LYP) supplemented with the standard 6-31G(d) and LANL2DZ basis set [14]. The optimized geometry corresponding to the minimum on the potential energy surface has been obtained by solving self-consistent field equation iteratively.

2.5 Antibacterial Activity

Antibacterial activity of Schiff base ligands and their mononuclear nickel(II) complexes (1-6) were tested against Gram negative (Escherichia coli, Klebsiella pneumoniae and Vibrio cholera) and Gram positive (Staphylococcus aureus) bacterial strains by agar well diffusion method [15]. Ciprofloxacin and Streptomycin (100 µg/mL) were used as standards. All discs and materials were sterilized in an autoclave before the experiments. Nutrient agar was used as sources for culturing bacterium at 37 $^{\circ}\text{C}$ on a rotary platform in an incubator. The ingredients were dissolved in distilled water and sterilized at 121 °C at 15 lbs for 15 min. Nutrient agar medium was prepared and plated aseptically into the sterile plates. Bacterial inoculums were prepared by growing a single colony overnight in nutrient broth and made a lawn culture using sterile swab over the nutrient medium plates. After the lawn preparation, discs impregnated with the ligand and complexes at different concentrations (25–100 $\mu g/mL$) and DMSO (control) was placed on the petriplates using sterile forceps and sonicated to ensure optimum nanoparticle dispersion using a sonicator bath at room temperature for 15 minutes to avoid the nanoparticles agglomeration. After incubation for 24 h at 37 °C, a clear zone around the discs was an evidence of antibacterial activity. From this clear zone, the inhibition zone was measured.

2.6 In Vitro Antioxidant Activity

The antioxidant activity of the synthesized mononuclear nickel(II) complexes were studied using standard methods. The concentration of the

complexes, and standard solutions used were 1.56–100 μ g/mL. The absorbance was measured spectrophotometrically against the corresponding blank solutions. The percentage of inhibition was calculated by using the following formula,

Radical scavenging activity (%) = (OD control – OD sample/OD control) × 100

2.6.1 ABTS Free Radical

2,2'-Azino-bis(3-ethylbenzothiazoline-6-sulphonic acid) (ABTS) (54.8 mg, 2 mM) was dissolved in 50 mL of distilled water and potassium persulphate (0.3 mL, 17 mM) was added. The reaction mixture was left to stand at room temperature overnight in dark before usage. To 0.2 mL of various concentrations of the samples/standard added 1.0 mL of freshly distilled DMSO and 0.16 mL of ABTS solution to make a final volume of 1.36 mL. After 20 min, absorbance was measured spectrophotometrically at 734 nm [16].

2.6.2 DPPH Free Radical

The assay was carried out in a 96 well microtitre plate. To 200 μL of DPPH solution, 10 μL of each of the samples or standard solution was added separately in wells. The plates were incubated for 30 min at 37 °C, and the absorbance was measured at 490 nm [17].

2.7 Molecular Docking Studies

A molecular docking study was carried out by the AutoDock Tools (ADT) version 1.5.6 and AutoDock version 4.2.5.1 docking programs. The structure of present complexes (1-6) was converted into PDB format from mol format using OPENBABEL. The crystal structure of the BSA (PDB ID: was downloaded from the protein data (http://www.rcsb.org./pdb). Receptor (BSA) and ligand (complexes) files were set using AutoDock Tools. Initially, all the heteroatoms with water molecules were deleted and polar hydrogen atoms and Kollman charges were additional to receptor molecule, then rotatable bonds in complexes were assigned. Remaining bonds were allowed to rotate. The BSA was covered in a box with number of grid points in x × y × z directions, 110 × 110×110 and a grid spacing of 0.4 Å. Lamarckian genetic algorithm, as implemented in AutoDock, was working to carry out docking calculations. Residual parameters were defaulting settings. For every docking case, the lowest energy docked conformation, according to the AutoDock scoring function, was selected as the binding mode. Visualization of the docked position has been done by using PyMOL molecular graphics program.

2.8 Anticancer Activity

2.8.1 MTT Assay

The anticancer activity of complexes (1–6) were tested against human breast cancer cell line (MDA-MB-231) and normal human dermal fibroblast cell line (NHDF) by MTT assay after 48 h treatment [18]. The MDA-MB-231 cells were grown in DMEM medium containing 10% FBS. For screening experiments, the cells (1 × 10^5 cells/well) were plated in 96-well plates with the medium containing 10% FBS and incubated for 24 h under CO_2 at 37 °C. Later, the medium was replaced with DMEM containing 1% FBS and the complexes (10–250 μ M) dissolved in 0.05% DMSO were added to the cells incubated at 37 °C in 5% CO_2 . After treatment, the plates were incubated for 24 h in order to perform cytotoxic analysis using MTT assay. 10 μ L of MTT (5 mg/mL) was added to each well and incubated for 4 h. Purple color farmazone crystals formed were then dissolved in dimethylsulfoxide (100 μ L). These crystals were observed at 570 nm in a multi well ELISA plate reader. The cell viability (%) was evaluated using the following equation:

Cell viability (%) = $(A_{570 \text{ nm}} \text{ of treated cells}/A_{570 \text{ nm}} \text{ of control cells}) \times 100$

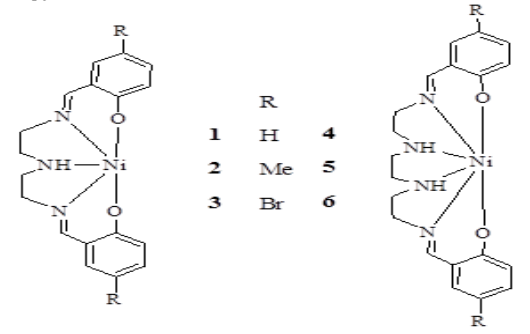
2.8.2 AO/EB and Hoechst 33258 Staining Assay

To evaluate the morphological changes of complexes (1–6) using MDA-MB-231 cell lines with acridine orange (AO) and ethidium bromide (EB), and Hoechst 33258 staining methods. The cells seeded in 96-well plates (37 °C, 5% CO₂). The medium was removed and replaced with the complexes (25 μ M). After 48 h, the cells were washed in phosphate-buffered saline (PBS) and stained with 40% paraformaldehyde and AO/EB, and Hoechst 33258 (10 mg/mL) at room temperature. Morphological evaluations of nuclear condensation and fragmentation were performed immediately after staining by means of fluorescent microscope (Olympus, Japan) at 550 nm of emission.

3. Results and Discussion

3.1 Synthesis and Spectral Characterization

The Schiff base ligands (L^{1-6}) and their mononuclear nickel(II) complexes (1–6) have been synthesized using general procedure and obtained in good yield (Scheme 1). The authenticities of complexes were determined by elemental analysis, FT IR, UV-Vis, CV, EPR and ESI mass spectroscopy.

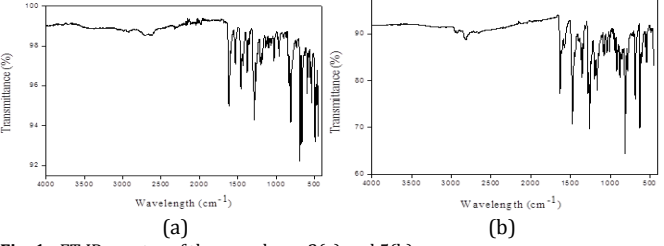


Scheme 1 Mononuclear nickel(II) complexes

3.2 Spectral Characterization

FTIR spectra (Fig. 1a) of all the ligands show a broad centered band in the region 3532–3547 cm $^{-1}$ due to the phenolic O–H stretching, which is disappeared on the addition of metal ion indicates the formation of complexes. At the same time, the phenolic C–O stretching vibration of ligands increases (1348–1361 cm $^{-1}$) upon complexation (1376-1389 cm $^{-1}$) suggest the coordination of phenolic group with nickel ion via deprotonation. All the ligands exhibit a sharp band in the region 1641–1630 cm $^{-1}$ due to the azomethine linkage v(C=N) was shifted towards lower frequency 1628–1612 cm $^{-1}$ for complexes clearly indicates the coordination of azomethine nitrogen with metal(II) ion. All the complexes show a medium intensity bands in the region 2968–2949 cm $^{-1}$ and 1584–1569 cm $^{-1}$ due to N–H stretching and twisting frequency of ligands (Fig. 1a). The new and non-ligand medium intensity bands were seen in the region 524–502 and 461–428 cm $^{-1}$ due to v(Ni–O) and v(Ni–N) vibrations, respectively.

The UV-Vis absorption spectra of all the complexes (1–6) were recorded in MeOH medium, which gives more suitable information about their geometrical properties. The complexes show intense band in the range 236–278 nm is assigned to an intra-ligand charge transfer $(\pi-\pi^*)$, while the moderately intense band was observed in the range 348–376 nm is due to the charge transfer from the phenol oxygen to the Ni(II) ion. Finally, the complexes (1–3) display a broad band in the range 642–661 nm because of a metal-centered d–d transition, which suggests square-pyramidal geometry around the nickel(II) ion [19], whereas the complexes (4–6) show a broad band in the range 608–621 and 910–918 nm is due to d–d transition, which suggests distorted octahedral geometry around the nickel(II) ion [20].



 $\textbf{Fig. 1a} \; \text{FT IR spectra of the complexes 2(a) and 5(b)}$

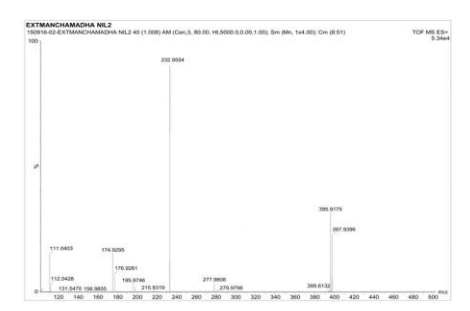


Fig. 1b ESI mass spectrum of complex 2

The mass spectra (Fig. 1b) of complexes have been examined in positive mode and they exhibit molecular ion peak of corresponding complexes, which prove the formation of complexes. The obtained molecular ion peaks are comparable with their molecular weight. The observed mass data clearly demonstrate the proposed molecular formulae of the complexes.

3.3 Electrochemical Properties

The electrochemical properties of redox active nickel(II) complexes (1–6) were evaluated by cyclic voltammetry in the potential range +1.4 to -1.4 V in DMF containing 0.1 M tetra(n-butyl)-ammonium perchlorate.

3.3.1 Reduction Process

All the complexes display an irreversible one electron transfer process in between –0.82 and –0.99 V, which can be assigned to the reduction of the metal(II) ion centre (Fig. 2). The reduction capability of complexes 3 and 6 is less negative with respect to other complexes, which demonstrates that the +1 oxidation state is more balanced out in complexes 3 and 6 than other complexes. The reduction process can be assigned as follows:

$$Ni(II) \leftrightarrow Ni(I)$$

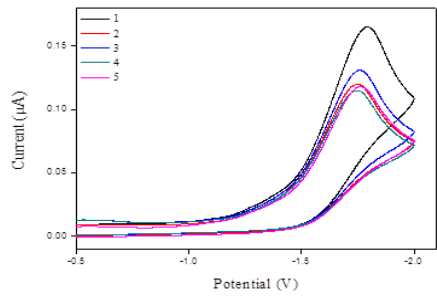


Fig. 2 Reduction voltammograms of nickel(II) complexes

3.3.2 Oxidation Process

All the complexes display an irreversible one electron transfer process in between +1.15 to +1.4 V for oxidation process, which can be assigned to the oxidation of the metal(II) ion centre (Fig. 3). The oxidation capability of complexes 2 and 5 is more positive with respect to other complexes. The oxidation process can be assigned as follows:

$$Ni(II) \leftrightarrow Ni(III)$$

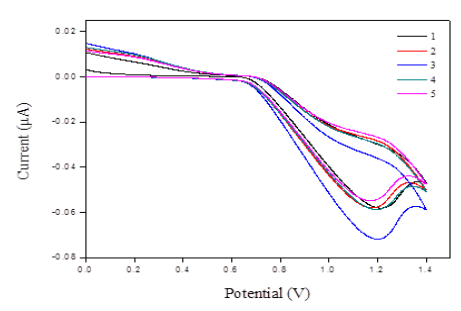


Fig. 3 Oxidation voltammograms of nickel(II) complexes

3.4 Geometry Optimization

DFT calculation is a tool of expanding significance for the structural investigation of coordination and organometallic complexes. In the absence of crystal data, DFT calculations provide more suitable information about geometrical properties. Taking into consideration, the mononuclear nickel(II) complexes (1-6) were optimized at B3LYP/LANL2DZ levels in gas phase and the optimized ground state geometry structures are shown in Figs. 4 and 5. The calculated bond lengths and angles of the complexes are listed in Table 1. The five coordinated complexes (1-3), coordinate through two phenolic oxygen, two azomethine nitrogen and one primary -NH atoms. The observed Ni-O and Ni-N bond lengths of the complexes (1-3) observed in the range from $2.198\ to\ 2.0601\ \mbox{\normalfont\AA}$ and $2.3743\ to\ 2.0343\ \mbox{\normalfont\AA}$, respectively, which is more consistent with previously reported work [21, 22]. The combined B3LYP method and LANL2DZ basis gives a tremendous evaluation of Ni(II) to N and O bond distances, Ni-N1, Ni-N2, Ni-O1and Ni-O2. Molecular geometries can be predicted by calculating τ values using the equation [23].

 $\tau = \beta - \alpha/60$

where α and β are the equatorial and axial bond angles, respectively. Generally, if the molecular geometry is square pyramidal, τ value is close to 0, while if τ value is close to 1 then the geometry is similar to trigonal bipyramidal. For complexes (1–3) α (NH–Ni–O(2) values are 109.14, 110.36 and 112.13, respectively and β (NH(2)–Ni–O(1) values are 108.12, 110.12 and 110.09, respectively. The observed results indicate the complexes (1–3) as their τ values is equal to 0, which indicate the distorted square pyramidal geometry around nickel(II) center. The six coordinated complexes (4–6) coordinate through two phenolic oxygen, two azomethine nitrogen and two primary –NH atoms.

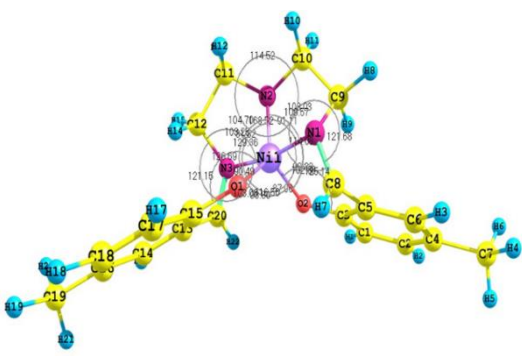
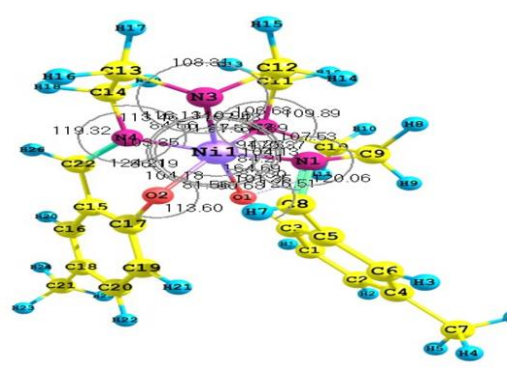


Fig. 4 The optimized structure complex 2 at the B3LYP/LANL2DZ level



 $\textbf{Fig. 5} \ \text{The optimized structure complex 5 at the B3LYP/LANL2DZ level}$

Table 1 B3LYP/LANL2DZ bond lengths (Å) and bond angles (°) of nickel(II) complexes (1-6)

Parameters	Calculated B3LYP/LANL2DZ						Experimental	
	1	2	3	4	5	6	Experimental	
Bond length (Å)								
Ni-N(1)	2.112	2.034	2.187	2.109	2.143	2.148	2.055	
Ni-N(2)	2.374	2.367	2.356	2.343	2.358	2.364	2.359	
Ni-O(1)	2.061	2.018	2.021	2.036	2.018	2.040	2.062	
Ni-O(2)	2.194	2.198	2.192	2.193	2.103	2.193	2.117	
Ni-NH(1)	2.211	2.214	2.208	2.214	2.214	2.218	-	
Ni-NH(2)	2.321	2.307	2.306	2.317	2.312	2.319	-	
Bond angle (°)								
O1-Ni-N1	108.54	107.11	108.17	107.46	106.11	106.53	-	
O1-Ni-NH1	109.14	111.03	111.32	117.47	114.36	115.46	-	
O1-Ni-NH2	-	-	-	78.65	78.44	76.67	-	
01-Ni-02	161.32	161.926	159.25	160.43	161.74	160.78	-	
O1-Ni-N2				132.28	129.58	132.74		
N1-Ni-NH1	124.23	124.64	125.57	125.35	123.26	123.37	-	
N1-Ni-NH2	-	-	-	110.75	110.28	108.27	-	
N1-Ni-N2	168.65	165.79	166.98	166.36	167.16	168.22	-	
N1-Ni-02	-	-	-	112.57	112.08	110.64	-	
NH1-Ni-				141.32	139.75	139.25		
NH2	_	_	_	141.32	137.73	137.23	-	
NH1-Ni-N2	91.11	89.13	90.12	96.22	98.15	97.77	-	
NH1-Ni-02	108.34	109.09	110.46	118.15	113.29	116.35	-	
N2-Ni-02	-	-	-	128.98	127.42	120.16	-	
N2-Ni-N1	-	-	-	140.10	149.25	149.53	-	
N2-Ni-NH2	-	-	-	96.22	97.27	96.21	_	

3.5 Biological Evolutions

3.5.1 Antibacterial Activity

Generally, metal complexes are more dynamic than ligands as they may serve as central cytotoxic species. In this way, they exhibit wide range nature and can be further utilized as a part of pharmaceutical industry for humankind, as an antimicrobial agent, in the wake of testing its toxicity to

people. In this regard, we are interested to evaluate the In vitro antibacterial activity of mononuclear nickel(II) complexes (1-6) were tested against three Gram negative (Escherichia coli, Klebsiella pneumoniae and Vibrio cholera) and one Gram positive (Staphylococcus aureus) strains by agar well diffusion method. The antibacterial activity of the complexes has been found to be significant efficiency than the corresponding ligands at the measured concentrations. The positive control (Ciprofloxacin) produces remarkable sized inhibition zones against the tested bacteria however negative control (DMSO) creates no discernible inhibitory impact against any of the test organisms. Tested complexes demonstrated zone of inhibition ranging 10-19 mm against the Gram positive microorganisms and between 9 to 18 mm against Gram-negative microorganisms. The Schiff base ligands (L1-6) show zone of inhibition ranging 6.1-15.8 mm against Gram positive microorganisms and 5.7-14.8 mm against Gram negative microorganisms. It has been noticed that the metal complexes established expanded zone of inhibition against the bacterial strains when contrasted with their corresponding ligands ranging 10.4-21.2 mm. From the zone of inhibition, all the complexes show higher activity against Gram positive than Gram negative bacteria. Complex 5 was observed to be best active agent against E. coli, K. pneumoniae, V. cholera and S. Aureus with the zone of inhibition of 19, 21.5, 16.9 and 17.4 mm, respectively.

3.5.2 Antioxidant Activities

The In vitro antioxidant ability of the complexes (1-6) was tested by ABTS and DPPH free radical scavenging assay method using ascorbic acid and butylated hydroxyl toluene (BHT) as standard. Generally, ABTS is a long-life ABTS⁻⁺ radical cation and DPPH is more stable radical, which react with any compound that supply an electron or hydrogen atom, resulting in a colour change from purple to yellow. The antioxidant activity of the complexes was tested at different concentrations (25-100 µg/mL). IC₅₀ values has observed from the plots of percentage of inhibition with an increase in concentration of the complexes (Fig. 6), and observed IC₅₀ values are listed in Table 1. As seen from results, the complexes 2 and 5 show higher scavenging ability than standard drugs such as ascorbic acid and BHT (Table 2). The antioxidant activity follows the order 5>2> ascorbic acid > BHT > 4>2>6>3. Importantly, the complexes 2 and 5 show better antioxidant activity over to other complexes, which may be attributed to the significant contribution of the methyl substituent [24]. The observed higher antioxidant activity of the metal complexes depend on the nature of geometry, ionization potential, reactivity, reducing capacity and including conjugation [25].

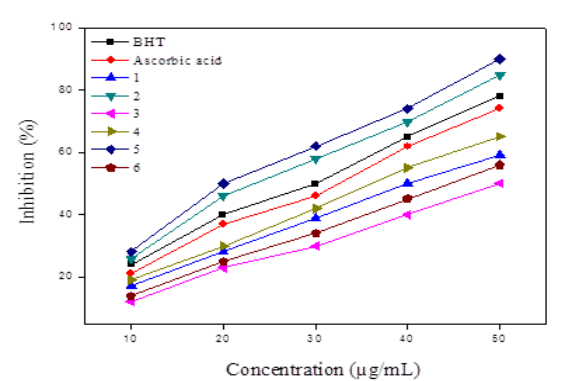


Fig. 6 In vitro DPPH radical scavenging activity of complexes

Table 2 In vitro antioxidant and anticancer activity of complexes (1-6)

Complexes/	IC ₅₀ value (μg,	value (µg/mL)				
Standards	ABTS	DPPH	MDA-MB-231	NHDF		
1	22.17 ± 0.21	22.16 ± 0.15	24.22 ± 0.43	>100		
2	16.09 ± 0.11	12.47 ± 0.72	17.11 ± 0.14	>100		
3	25.34 ± 1.10	29.92 ± 1.73	28.23 ± 0.13	>100		
4	19.18 ± 0.21	19.91 ± 1.09	21.07 ± 0.21	>100		
5	14.24 ± 0.12	10.17 ± 0.74	15.42 ± 0.21	>100		
6	21.45 ± 0.09	27.17 ± 1.10	25.48 ± 0.87	>100		
Ascorbic acid	18.12 ± 0.66	14.23 ± 0.88	-	-		
BHT	17.16 ± 0.29	13.09 ± 0.63	_	-		
Cisplatin	-	-	19.16 ± 1.08	>100		

3.5.3 Molecular Docking with EGFR Kinase Receptor

All the complexes are mostly located in active site of the EGFR kinase receptor are shown in Fig. 7, and the observed free binding energy values are listed in Table 3. The complexes 2 and 5 effectively bind to EGFR kinase receptor via π – π , σ – π , hydrogen bonding, electrostatic and van der Waals interactions.

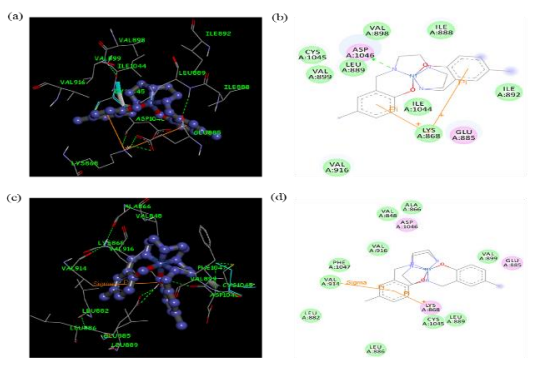


Fig. 7 3D and 2D molecular docking interaction of complexes 2 (a, b) and 5 (c, d) with EGFR kinase receptor (PDB ID: 1M17)

Complex 2 was stabilized by one hydrogen bond interaction formed between hydrogen atom of Asp1046 and azomethine nitrogen atom (bond length: H···N = 3.1 Å), which also show two π - π interaction formed between the two phenol ring and Lys868 (bond length: 3.7 and 3.6 Å). The electrostatic interaction formed between the complex and residues Glu885 and Asp1046, and van der Waals interaction formed between complex and residues Lys868, Ile888, Leu889, Ile892, Val898, Val899, Ile1044 and Asp1046. Complex 5 shows one π - π interaction formed between the phenol ring and Lys868 (bond length: 3.6 Å), which also shows one σ - π interaction formed between the phenol ring and Val914 (bond length: 3.6 Å). The electrostatic interaction formed between the complex and residues Lys868, Glu885 and Asp1046, and van der Waals interaction formed between complex and residues Val848, Ala866, Leu882, Leu886, Leu889, Val899, Val914, Val916, Cys1045 and Phe1047. The observed data indicate EGFR kinase receptor as the significant inhibitor for all the complexes, because all the complexes were retained tightly by the binding pocket of EGFR.

 $\textbf{Table 3} \ \ \text{Molecular docking parameters of the complexes (1-6) with EGFR kinase receptor$

Com plexe s	Final interm energy (kcal vdW + H bond + dissolving		Total (1)	Final total internal energy (kcal mol ⁻¹)	Torsio nal free energy (kcal mol ⁻¹) (3)	Unbou nd system 's energy (kcal	Estimate d free energy of binding [(1)+(2)+(3) -
	energy					mol-1)	(4)](kcal
				(2)	(3)	(4)	mol-1)
1	- 5.18	-0.12	- 5.30	+0.00	+0.00	+0.00	- 5.30
2	- 7.01	- 0.11	- 7.12	+0.00	+0.00	+0.00	- 7.12
3	- 4.23	-0.11	- 4.34	+0.00	+0.00	+0.00	- 4.34
4	- 6.13	- 0.03	- 6.15	+0.00	+0.00	+0.00	- 6.15
5	- 7.94	- 0.05	- 7.99	+0.00	+0.00	+0.00	-7.99
6	- 5.03	-0.04	- 5.07	+0.00	+0.00	+0.00	- 5.07

3.5.4 MTT Assay

In vitro anticancer activity of complexes (1–6) was tested against human breast cancer cell line (MDA-MB-231) and normal human dermal fibroblast cell line (NHDF) by MTT assay after 48 h treatment. The potential anticancer drug (cisplatin) was used as the standard positive control. The IC $_{50}$ values were listed in Table 2. The cell viability was concentration dependent, with increasing complex concentrations and decrease in cell viability. All the complexes show superior potency to cancer cell line (MDA-MB-231), also all the complexes (1–6) exhibit less toxic in normal cell line (NHDF). The observed data reveal good anticancer activity of the complexes 2 and 5 against MDA-MB-231 cancer cell lines, compared to cisplatin. The higher activity of these complexes is due to electron releasing groups in para position, which increase in lipophilicity and hydrophobic interactions.

3.5.5 Apoptosis by Hoechst 33258 Staining Assay

Apoptosis induction is one of the conceptions in the development of drug; many anticancer drugs in present use were showed to induce apoptosis in susceptible cells [26]. In order to understand the type of cell death induced by Ni(II) complexes was tested on MDA-MB-231 cells stained with Hoechst 33258. After the treatment of complexes for 48 h, the results show the morphological changes such as fragmentation of chromatin, cell shrinkage, plasma membrane blebbing, cytoplasmic vacuolation, nuclear fragmentation and nuclear swelling as compared to control cells (Fig. 8). These morphological changes indicate that the complexes induced either apoptosis or necrosis.

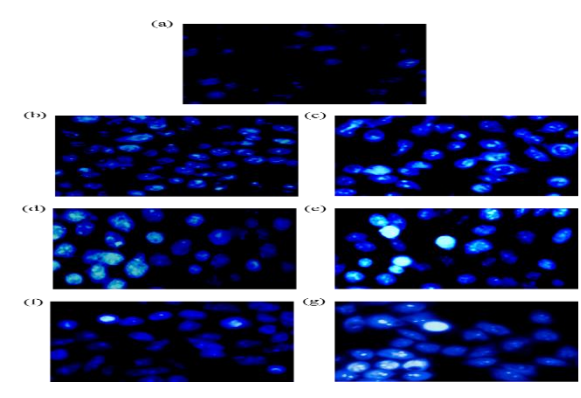


Fig. 8 Hoechst 33258 staining of EAC cells for 48 h: Control (a), 1 (b) 2 (c), 3 (d), 4 (e), 5 (f) and 6 (g)

3.5.6 Apoptosis by AO/EB Staining Assay

Further to sustain the morphological changes of nicke(II) complexes (1–6) with MDA-MB-231 cells was stained with acridine orange (AO) and ethidium bromide (EB) after treatment with the complexes for 48 h (Fig. 9). The control cells show bright green spot, whereas, the complexes (25 $\mu\text{M})$ treatment with MDA-MB-231 cells after stained with AO/EB the morphological was changed, the many cells become shrinkage, cell blebbing and chromatin condensation were observed. These data show that all the complexes induce apoptosis in the MDA-MB-231 cells.

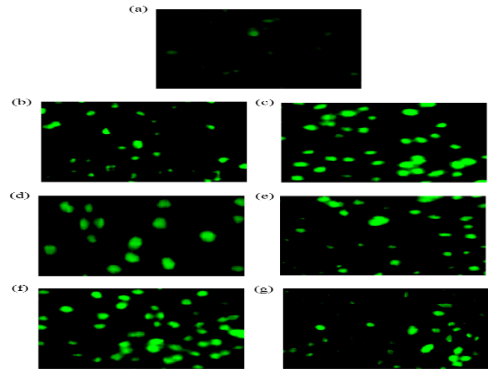


Fig. 9 AO/EB staining of EAC cells for 48 h: Control (a), 1 (b) 2 (c), 3 (d), 4 (e), 5 (f) and 6 (g)

4. Conclusion

A series of mononuclear nickel(II) complexes derived from Schiff base ligands have been successfully synthesized and fully characterized. The geometry of the complexes 1–3 show square pyramidal and the other three complexes 4–6 show distorted octahedral geometry around Ni(II) ion. DFT calculations used to predict the molecular geometry of the complexes. All the complexes show pronounced antibacterial activity and also they display significant antioxidant activity with respect to standard drugs. The complexes strongly interact with epidermal growth factor receptor (EGFR). *In vitro* anticancer activity of the complexes shows comparable activity to the cisplatin against the same cancer cell lines. The methyl substituted complexes 2 and 5 show higher anticancer activity when compared to other complexes. The morphological assessment data observed from Hoechst 33258 and AO/EB staining assays exhibit that the complexes induce the cancer cell death through apoptosis.

Acknowledgement

The authors are grateful to Sophisticated Analytical Instruments Facility (SAIF), Indian Institute of Technology Madras (IIT-M), Chennai 600 036, for ESI MS studies. Author KM thankful to Dr. P. Gurumoorthy, Assistant Professor, Department of Chemistry, Sriram College of Arts and Science, Perumalpattu, Tiruvallur-602 024, for his help in the antioxidant studies.

References

 K. Singh, M.S. Barwa, P. Tyagi, Synthesis, characterization and biological studies of Co(II), Ni(II), Cu(II) and Zn(II) complexes with bidentate Schiff bases derived by heterocyclic ketone, Eur. J. Med. Chem. 41 (2006) 147-153.

- [2] P. Panneerselvam, R.B. Nair, G. Vijayalakshmi, E.H. Subramanian, S.K. Sridhar, Synthesis of Schiff bases of 4-(4-aminophenyl)-morpholine as potential antimicrobial agents, Eur. J. Med. Chem. 40 (2005) 225-229.
- [3] R. Mladenova, M. Ignatova, N. Manolova, T. Petrova, I. Rashkov, Preparation, characterization and biological activity of Schiff base compounds derived from 8-hydroxyquinoline-2-carboxaldehyde and Jeffamines ED®, Eur. Polym. J. 38 (2002) 989-999.
- [4] O.M. Walsh, M.J. Meegan, R.M. Prendergast, T.A. Nakib, Synthesis of 3-acetoxyazetidin-2-ones and 3-hydroxyazetidin-2-ones with antifungal and antibacterial activity, Eur. J. Med. Chem. 31 (1996) 989-1000.
- [5] X.M. Ouyang, B.L. Fei, T.A. Okamuro, W.Y. Sun, W.X. Tang, et al, Synthesis, crystal structure and (SOD) Activity of novel seven-cordinated Mg(II) complex with multidentate Di-Schiff base ligands, Chem. Lett. (2002) 362-363.
- [6] N. Raman, Y.P. Raja, A. Kulandaismy, Synthesis and characterization Cu(II), Ni(II), Mn(II), Zn(II) and Vo(II) Schiff base complexes, Proc. Ind. Acad. Sci. Chem. Sci. 113 (2001) 183-189.
- [7] C. Jayabalakrishnan, K. Natarajan, Ruthenium (II) carbonyl complexes with tridentate Schiff bases and their antibacterial activity, Trans. Met. Chem. 27 (2002) 75-79.
- [8] J. Chakraborty, R.N. Patel, Copper-, Cobalt- and zinc(II) complexes with monofunctional bidentate schiff base and monodentate neutral ligands, J. Ind. Chem. Soc. 73 (1996) 191-193.
- [9] P. Krishnamoorthy, P. Sathyadevi, R.R. Butorac, A.H. Cowley, N.S.P. Bhuvanesh, et al, Copper(I) and nickel(II) complexes with 1:1 vs. 1:2 coordination of ferrocenyl hydrazone ligands: do the geometry and composition of complexes affect DNA binding/cleavage, protein binding, antioxidant and cytotoxic activities?, Dalton Trans. 41 (2012) 4423-4436.
- [10] J.J. Wang, L.Y. Wang, K. Zheng, Y.T. Li, C.W. Yan, et al, Synthesis and structure of a new trinuclear nickel(II) complex bridged by N-[3-(Dimethylamino)propyl]-N'-(2-hydroxyphenyl)oxamido: In vitro anticancer activities, and reactivities toward DNA and protein, J. Biochem. Mol. Toxicol. 31 (2017) 1-11.
- [11] S.J. Kirubavathy, R. Velmurugan, B. Tamilarasan, R. Karvembu, N.S.P. Bhuvanesh, et al, Synthesis, characterization, single-crystal XRD, and biological evaluation of nickel(ii) salen sulfadiazine complex, Synth. React. Inorg. Met. Org. Nano-Metal Chem. 46 (2016) 1751-1758.
- [12] C.K. Modi, I.A. Patel, B.T. Thaker, Manganese(III) Schiff-base complexes involving heterocyclic β-diketone and diethylene triamine, J. Coord. Chem. 61 (2008) 3110-3121.
- [13] M.J. Frisch, G.W. Trucks, H.B.H. Schlegel, G.E. Scuseria, M. Robb, et al, Gaussian 03 (Revision A.9), Gaussian, Inc., Pittsburgh, 2003.

- [14] A.D. Becke, Density-functional thermochemistry III, The role of exact exchange, J. Chem. Phys. 98 (1993) 5648-5652.
- [15] I. Ahmad, A.Z. Beg, Antimicrobial and phytochemical studies on 45 Indian medicinal plants against multi-drug resistant human pathogens, J. Ethnopharmacol. 74 (2001) 113-123.
- [16] R. Re, M. Pellegrini, A. Proteggente, A. Pannala, M. Yang, et al, Antioxidant activity applying an improved ABTS radical cation decolorization assay, Free Radic. Biol. Med. 26 (1999) 1231-1237.
- [17] N.T.T. Huong, K. Malsumato, R. Kasai, K. Yamasaki, H. Watanabeth, In vitro antioxidant activity of Vietnamese ginseng saponin and its components, Biol. Pharm. Bull. 21 (1998) 978-981.
- [18] T. Mosmann, Rapid colorimetric assay for cellular growth and survival: application to proliferation and cytotoxicity assays, J. Immunol. Methods 65 (1983) 55-63.
- [19] S.S. Massoud, F.R. Louka, R.N. David, M.J. Dartez, Q.L. Nguyn, et al, Five-coordinate metal (II) complexes based pyrazolyl ligands, Polyhedron 90 (2015) 258-265.
- [20] P.P. Netalkar, S.P. Netalkar, V.K. Revankar, Synthesis, crystal structures and characterization of late first row transition metal complexes derived from thiosemicarbazone hub: DNA binding/cleavage studies, Appl. Organometal. Chem. 29 (2015) 280-289.
- [21] J. Ravichandran, P. Gurumoorthy, C. Karthick, A. Kalilur Rahiman, Mononuclear zinc(II) complexes of 2-((2-(piperazin-1-yl)ethylimino)methyl)-4-substituted phenols: Synthesis, structural characterization, DNA binding and cheminuclease activities, J. Mol. Struct. 1062 (2014) 147-157.
- [22] P. Gurumoorthy, J. Ravichandran, A. Kalilur Rahiman, Mixed-ligand binuclear copper(II) complex of 5-methylsalicylaldehyde and 2,2'-bipyridyl: Synthesis, crystal structure, DNA binding and nuclease activity, J. Chem. Sci. 126 (2014) 783-792.
- [23] R.C. Charles, K.M. Geiser-Bush, S.P. Rowley, P.D. Boyle, Structural and electron paramagnetic resonance studies of the square pyramidal to trigonal bipyramidal distortion of vanadyl complexes containing sterically crowded Schiff base ligands, Inorg. Chem. 36 (1997) 6401-6408.
- [24] G. Dehghan, Z. Khoshkam, Tin(II)-quercetin complex: synthesis, spectral characterisation and antioxidant activity, Food Chem. 131 (2012) 422-426.
- [25] S.A.A. Nami, M. Alam, A. Husain, M. Parveen, Synthesis, characterization, thermal and antioxidant studies of potassium dihydrobisphenothiazinyl borate and its transition metal complexes, Spectrochim. Acta Part A 96 (2012) 729-735
- [26] J.A. Hickman, Apoptosis induced by anticancer drugs, Cancer Metastasis Rev. 11 (1992) 121-s139.